POLITECNICO DI TORINO
Repository ISTITUZIONALE

Numerical Study of Thin-Film Quantum-Dot Solar Cells Combining Selective Doping and Light-Trapping Approaches

Original
Numerical Study of Thin-Film Quantum-Dot Solar Cells Combining Selective Doping and Light-Trapping Approaches / Cappelluti, Federica; Gioannini, Mariangela; Ghione, Giovanni; Khalili, Arastoo. - ELETTRONICO. - (2016), pp. 1282-1286. (Intervento presentato al convegno 43th IEEE Photovoltaic Specialist Conference tenutosi a Portland, Oregon, USA nel 5-10 Giugno 2016) [10.1109/PVSC.2016.7749821].

Availability:
This version is available at: 11583/2657924 since: 2017-09-20T10:19:06Z

Publisher:
IEEE

Published
DOI:10.1109/PVSC.2016.7749821

Terms of use:

This article is made available under terms and conditions as specified in the corresponding bibliographic description in the repository

Publisher copyright

(Article begins on next page)

12 October 2024

Numerical Study of Thin-Film Quantum-Dot Solar Cells Combining Selective Doping and Light-Trapping Approaches

Federica Cappelluti, Mariangela Gioannini, Giovanni Ghione, Arastoo Khalili

Department of Electronics and Telecommunications, Politecnico di Torino, Torino, 10129, Italy

***Abstract*—We investigate GaAs-based quantum dot (QD) solar cells that exploit selective QD doping to mitigate open circuit voltage loss and light trapping enhancement of QD harvesting to increase the QD contribution to short-circuit current. Devices are simulated using an ad hoc developed physics-based model that accurately describes QD carrier dynamics within a semi-classical semiconductor transport model. The study of a realistic device structure under different hypotheses of crystal quality allows the impact of doping on device performance to be assessed both in radiative limited and non-radiative limited cases. We show that large open circuit voltage recovery is attainable in both cases due to the simultaneous suppression of radiative recombination through QD confined states and of non-radiative recombination in the barrier material, thus confirming the use of selective doping as a good strategy for optimizing QDSC design. Then, we study thin-film QDSCs that combine selective doping with light trapping approaches. The efficiency enhancement allows the QD cell to overcome the bulk reference one even under unconcentrated light.**

***Index Terms*—solar cell, quantum dot, thin film, doping, light trapping, GaAs, intermediate band.**

I. Introduction

The use of quantum dots in III-V solar cells is an attractive technology to enhance the power conversion efficiency of both single- and multi-junction solar cells and to pursue the practical implementation of the intermediate band (IB) solar cell [1]. Despite the promising theoretical predictions, reported InAs/GaAs QD solar cells have shown limited improvement of short circuit current (J_{sc}) and significant reduction of the open circuit voltage (V_{oc}), yielding overall performance well below the expectations. The small improvement in J_{sc} is inherently related to the small optical absorption cross-section of the QDs and to the technological limitations in terms of achievable QD density and number of QD layers in practical devices. One promising solution to boost the QD light absorption is to exploit photonic light trapping in thin-film structures [2] wherein, after substrate removal, nanostructured gratings can be monolithically integrated on the front and rear surface of the cells allowing for effective light trapping of long wavelength light [3], [2]. V_{oc} degradation involves the competition between optical and thermal escape, capture and radiative recombination through the QDs, and non-radiative recombination associated to defect formation during the QD growth. Selective QD doping, by modulation doping and direct doping techniques, has been proposed to suppress QD-barrier thermal coupling and mitigate recombination loss [4], [5], [6]. Experiments have demonstrated significant V_{oc} recovery using this approach but the interpretation of measured data is not straightforward due to the complicated interplay between recombination channels in the host material and QDs. In fact, in the prospect of optimized QD growth and high quality crystal QDSCs, it remains still unclear to what extent selective doping could improve the cell performance. In this framework, a deeper insight can be gained through physics-based models able to account for the peculiar QD carrier dynamics and their interplay with bulk carriers [7]. We have recently reported an extensive study on the influence of doping in simple GaAs based QD solar cells [8], showing that remarkable V_{oc} recovery can be expected by selective doping, regardless of the crystal quality. In this work we apply the methodology in [7], [8] to address the influence of QD selective doping in realistic solar cells structures and we investigate to what extent the efficiency of doped QDSCs may be enhanced by implementing light-trapping approaches within a thin-film cell configuration.

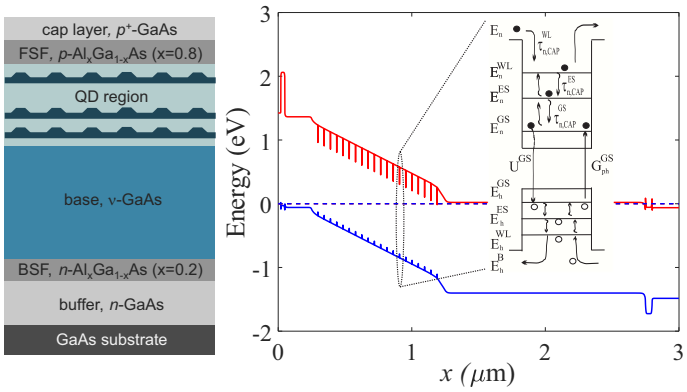

Fig. 1. Left: Sketch of the analyzed QD-based solar cell. Right: Calculated energy band diagram at thermal equilibrium. The inset shows the QD energy states and interband and intersubband transitions considered in the model.

II. Numerical Model and Analyzed Devices

A sketch of the analyzed QDSC structure is shown in Fig. 1: 20 QD layers are uniformly stacked in an intrinsic GaAs region placed between the p-type emitter and the n-type base. The device includes widegap window layers as front and back surface field layers. Geometrical, material, and doping parameters are reported in Table I.

As schematically described in Fig. 1, the model of the QD cell includes a drift-diffusion description of carrier transport in the bulk material and a set of phenomenological rate-equations (REs) for QD carrier dynamics [7]. QDs are

TABLE I
CELL STRUCTURE PARAMETERS

Layer	Thickness [nm]
cap layer, p^+ (10^{19} cm^{-3}) GaAs	20
FSF, p^+ (5×10^{18} cm^{-3}) $Al_{0.8}Ga_{0.2}As$	30
emitter, p^+ (10^{18} cm^{-3}) GaAs	200
QD region, i-GaAs	1000
base, n-GaAs (2×10^{17} cm^{-3})	1500
BSF, p^+ (5×10^{18} cm^{-3}) $Al_{0.2}Ga_{0.8}As$	50
buffer, n^+ (5×10^{18} cm^{-3}) GaAs	50
substrate, n^+ (5×10^{18} cm^{-3}) GaAs	300

described as a three-level system, including electron/hole ground state, excited state and the two dimensional wetting layer (WL) state. The QD rate equations and the continuity equations for barrier carriers are coupled through the escape (relaxation) rates of confined carriers towards (from) the barrier and the Poisson equation [7]. Relaxation and capture scattering times are set in a phenomenological way, by comparison with experimental results [7]. Escape time constants are linked to the capture/relaxation ones by the detailed balance at thermal equilibrium, under the hypothesis of thermal dominated escape. Thus, the strength of carriers escape from QD to barrier is connected to the QD band structure and in the present study is characterized by a marked asynchronism between holes and electrons. Purely radiative recombination is assumed through QDs. Interband optical generation is calculated from the QD absorption spectrum by accounting for electron and hole occupation in the QD states. A complete list of QD material parameters is summarized in Table II. Details on the used optical absorption spectra may be found in [8]. The model also accounts for barrier radiative recombination, with radiative coefficient set to 2.0×10^{-10} cm^{3}s^{-1}, and nonradiative recombination modeled according to Shockley Read Hall (SRH) theory, with carrier lifetimes ranging from 500 ns (high quality material, close to the radiative limit) down to 10 ns (defective material). All the presented simulations assume ambient temperature ($T = 300$ K).

TABLE II
QD PARAMETERS

Parameter definition	Value
Number of layers, N_L	20
QD density, N_{QD}, [cm^{-2}]	6×10^{10}
QD thickness, t_{QD}, [nm]	4
E_g^{WL}, E_g^{ES},E_g^{GS}, [eV]	1.33, 1.22, 1.13
Peak optical absorption, α_{WL}, α_{ES}, α_{GS}, [cm^{-1}]	2×10^4, 1800, 800
$\tau_{n,cap}^{B\text{-}WL}$, $\tau_{n,cap}^{WL\text{-}ES}$, $\tau_{n,cap}^{ES\text{-}GS}$, [ps]	0.3, 1, 1
$\tau_{p,cap}^{B\text{-}WL}$, $\tau_{p,cap}^{WL\text{-}ES}$, $\tau_{p,cap}^{ES\text{-}GS}$, [ps]	0.1, 0.1, 0.1
$\Delta E_n^{B\text{-}WL}$, $\Delta E_n^{WL\text{-}ES}$, $\Delta E_n^{ES\text{-}GS}$, [meV]	63, 96, 70
$\Delta E_p^{B\text{-}WL}$, $\Delta E_p^{WL\text{-}ES}$, $\Delta E_p^{ES\text{-}GS}$, [meV]	28, 16, 16

We consider as case study the direct doping method, modeled by placing 5 nm thick δ-doping layers at the QD layer. The sheet density of dopants is set to a multiple (α) of the QD density so as to nominally provide α carriers per dot. A bulk reference (REF) cell is also considered, where the QD region is replaced by a bulk GaAs region, with n-type doping of 1×10^{17} cm^{-3}, chosen to achieve the maximum efficiency.

III. RESULTS AND DISCUSSION

A. Photovoltage loss mitigation

Fig. 2 reports the V_{oc} dependence on doping density of the QD cell considering bulk SRH lifetimes of 500 ns and 10 ns. For the sake of comparison, the analysis is done also for the REF cell, where, given a nominal per-dot doping density α, the dopant density of the 1000 nm thick GaAs region (replacing the QD one) is calculated by conserving the total (per-unit-area) dopant dose of the δ-doped cells. The QD cells show very similar V_{oc} when undoped ($\alpha = 0$) and achieve comparable V_{oc} recovery with doping, regardless of barrier material quality. This demonstrates that QD radiative recombination is the dominant loss channel in the undoped cells and that doping effectively suppresses both the radiative and nonradiative recombination channels. In this regard, it is worth noting that a similar absolute improvement is achieved by the QD cell and the REF cell in the defective case ($\tau_{SRH} = 10$ ns).

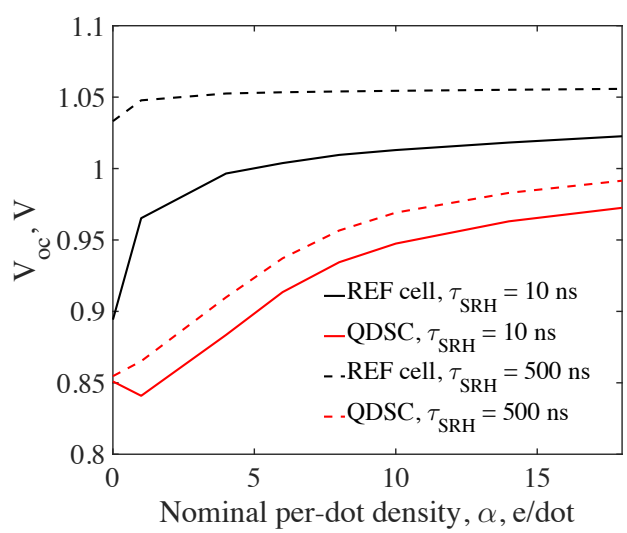

Fig. 2. Open circuit voltage as a function of the nominal per dot doping density for the reference cell and the n-type directly doped QD cell, assuming a defective barrier ($\tau_{SRH} = 10$ ns, solid lines) and a high quality barrier ($\tau_{SRH} = 500$ ns, dashed lines). In the reference cell, the actual doping level corresponds to $\alpha \times 1.2 \times 10^{16}$ cm^{-3}. The cell is simulated under 1 sun, AM1.5G illumination.

Thus, the analysis confirms selective doping as an effective strategy for mitigating V_{oc} penalty in both the ideal and

defective barrier case. At the highest doping density the estimated recovery ranges between 120-140 mV depending on the crystal quality and comparable results are also found for modulation doped cells (not shown here). The results are in good agreement with literature data, where the highest reported values are 121 mV for the 8e/dot modulation-doped cell in [9], and 105 mV for the 18e/dot directly doped cells in [10].

The residual V_{oc} penalty observed at the highest doping level must be attributed to the residual QD radiative recombination through the WL channel. This is evident by analyzing the open circuit photoluminescence (PL) spectra reported in Fig. 3: in the undoped cell the PL dominant peak is the GS one; as per-dot doping density increases, GS capture is suppressed and causes a slight increase of ES and WL PL; at the highest doping density the PL dominant contribution comes from the WL state.

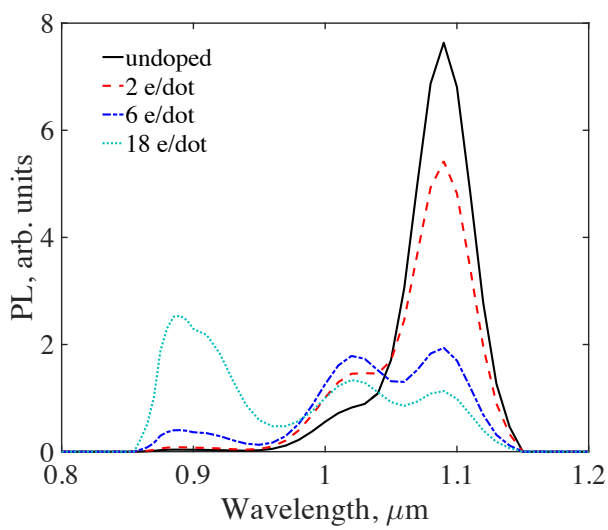

Fig. 3. PL spectra for undoped and doped QDSCs when $\tau_{SRH} = 10$ ns. The PL is calculated under barrier excitation at wavelength 532 nm with power density of 1.1 W/cm^2.

Doping has a remarkable effect also on the competition of the radiative and nonradiative recombination mechanisms that can be assessed through a detailed analysis of charge transfer processes across the different regions of the device [9], [8]. An overall - yet qualitative - picture can be gained by comparing the equivalent recombination currents in the active region at high voltages, where the cell operates close to flat band condition. Fig. 4, reports the evolution of the recombination rates (integrated across the QD and base regions) as the cell approaches the open circuit condition: in the undoped cell V_{oc} is limited by the QD radiative recombination, whereas SRH recombination remains smaller and confined to the space charge region, as highlighted by its larger ideality factor. In the directly doped cell, both radiative and SRH recombination are suppressed and contribute at a similar extent to the cell loss at open circuit.

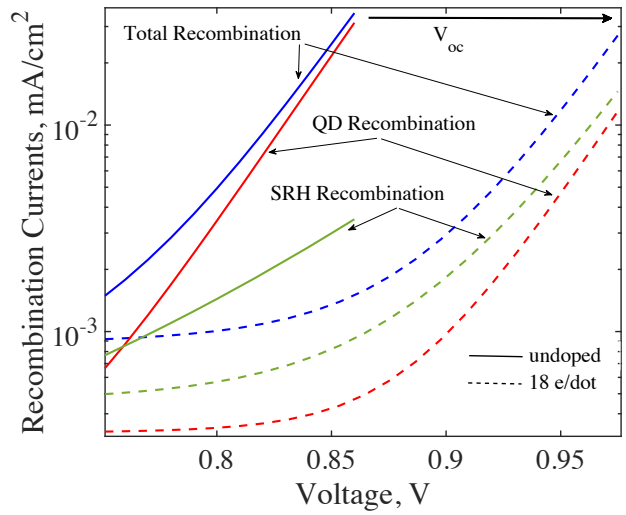

Fig. 4. Voltage dependence of the integrated recombination rates across the QD and base region (overall thickness of 2.5 μm) for the undoped and 18e/dot directly doped cell. Radiative recombination in the barrier, not shown here, is always negligible across the QD and base region. The voltage sweeps up to the V_{oc} of each cell, i.e. about 0.86 V and 0.97 V for undoped and doped cell, respectively.

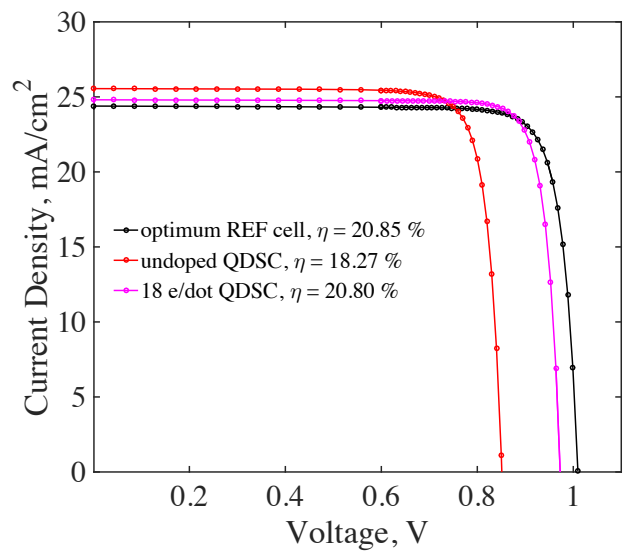

Fig. 5. $J-V$ characteristic under 1 sun AM1.5G illumination for optimum reference solar cell, undoped QD cell, and 18 e/dot QD cell.

Finally, the calculated I-V characteristics for the undoped and doped QD and REF cells are compared in Fig. 5. Thanks to the large V_{oc} recovery and slightly improved fill factor (see data summarized in table III), the 18 e/dot doped QDSC reaches a power conversion efficiency comparable with (yet slightly lower than) the reference cell one.

B. Photonically-enhanced thin-film cells

We now investigate if and to what extent the efficiency of the QD cells could outperform the bulk cell one when

effective light trapping is implemented at the GaAs bandedge and QD wavelengths. For this analysis we focus on the defective case study, with barrier lifetime set to 10 ns.

A schematic illustration of light trapping in the thin-film cell configuration is shown in Fig. 6. To model the light-trapping mechanism we follow the analytical approach in [11], [12]. As depicted in Fig. 6, the optical field in the cell results as the combination of downward and upward propagating fluxes, according to the following relationship:

$$\phi(x) = \phi^{\text{inc}}\,(1 - R_{\text{ext}})\,\frac{T^{+}(x) + R_{\text{b}}T^{+}(W)T^{-}(x)}{1 - R_{\text{b}}R_{\text{f}}T^{+}(L)T^{-}(0)} \qquad (1)$$

where R_{ext} is the reflectance at the illuminated surface, R_{b} the rear reflector reflectance, and R_{f} is the top internal reflectance that in the Lambertian light-trapping scheme results as $R_{\text{f}} = 1-(1-R_{\text{ext}})/n^2$, n being the semiconductor refractive index; T^{+} and T^{-} are the transmittance for the downward and upward propagating fluxes, respectively, calculated assuming perpendicular propagation, i.e. neglecting the light angular spreading induced by the Lambertian surface. Thus, in the presented simulations, the Lambertian limit of the average optical length enhancement approaches $2n^2$ (about 25 for GaAs), and it may be considered somewhat conservative with respect to the $4n^2$ limit expected in truly 3D geometries. The standing wave optical intensity distribution in eq. 1 is self-consistently calculated with the electrical equations, thus accounting for QD carrier filling (and associated optical absorption reduction) of the QD states. Fig. 7 compares the optical photogeneration rates at short-circuit conditions for the undoped QD cell in single pass and light-trapping (LT) configuration. It is well visible the enhancement of long wavelength light absorption in the bottom region of the cell as well as the enhancement of QD photogeneration. For the weakly absorbing GS state, the gain with respect to the single pass situation reaches the 25 limit.

The impact in terms of achievable short circuit current may be appraised in Fig. 8, where we compare the External Quantum Efficiency (EQE) spectra of undoped REF, undoped QD and doped QD cells for single-pass and light trapping configurations. The effect of light-trapping is well visible at the GaAs band edge and provides a remarkable EQE increase at QD wavelengths. The comparison between undoped and doped QD cell points out the suppression of GS and ES QD photogeneration due to the high doping level, however a significant increase of EQE with respect to the single pass cell can still be achieved in the WL range. In optimized designs a trade-off shall be sought for in terms of doping as well as of QD layers and density. Finally, the $J-V$ characteristics at 1 sun for the optimum REF cell, undoped and 18 e/dot QDSC are compared in Fig. 9, showing an absolute improvement of the efficiency of about 1.5 % for the light-trapping enhanced, doped QDSC with respect to the optimum baseline cell.

IV. Conclusion

We have studied through physics-based simulations the impact of selective doping and light trapping in InAs/GaAs

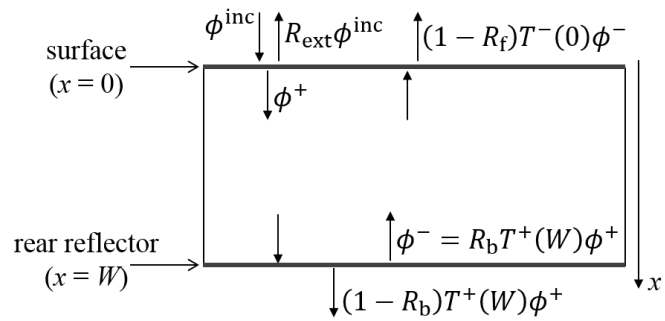

Fig. 6. Analysis of photon fluxes in the thin-film light-trapping cell.

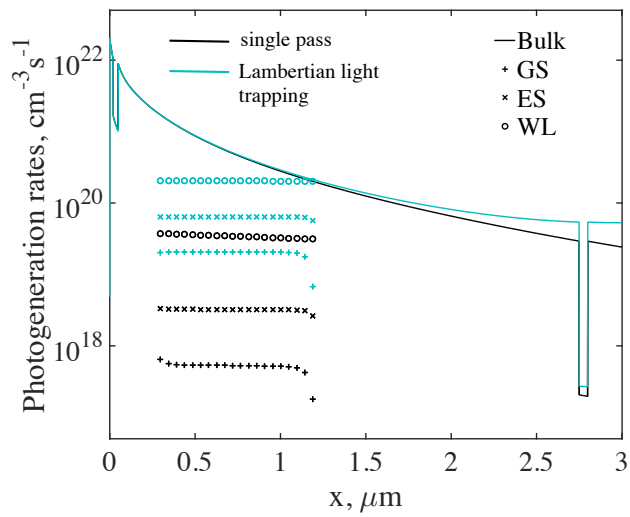

Fig. 7. Photogeneration rates in the single pass and light trapping configuration for the undoped QD cell, under 1 sun AM1.5G. The equivalent volume rates for QD states are computed by normalizing the corresponding surface rates by the QD layer interspacing.

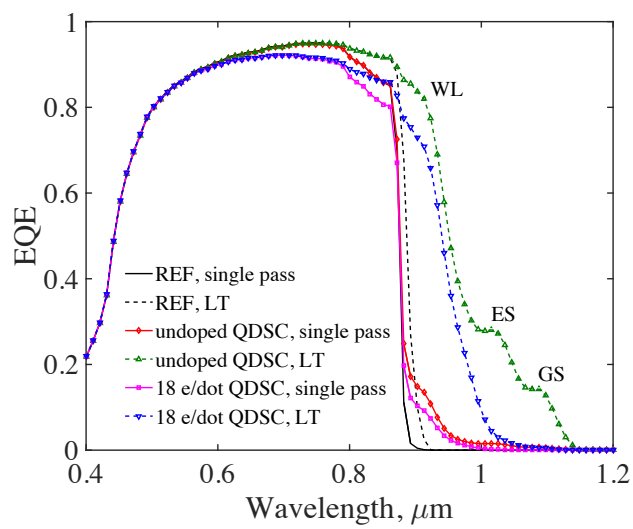

Fig. 8. EQE spectra of undoped reference cell, undoped QDSC, and directly doped 18 e/dot QDSC for single pass and light-trapping configuration.

TABLE III
SUMMARY OF THE PERFORMANCE OF THE SIMULATED CELLS

Cell type	**Photonic configuration**	**efficiency, %**	V_{oc}, **V**	J_{sc}, **mA/cm^2**	**FF**
undoped REF cell (intrinsic region replaces the QD one)	single pass	18.3004	0.8942	25.0560	0.8168
optimum REF cell	single pass	20.8533	1.0096	24.3838	0.8471
optimum REF cell	LT	21.5743	1.0106	25.1995	0.8472
QDSC undoped	single pass	18.2702	0.8511	25.5503	0.8402
QDSC 18 e/dot	single pass	20.8032	0.9727	24.8032	0.8623
QDSC undoped	LT	21.4682	0.8554	29.8088	0.8419
QDSC 18 e/dot	LT	23.1608	0.9757	27.5957	0.8602

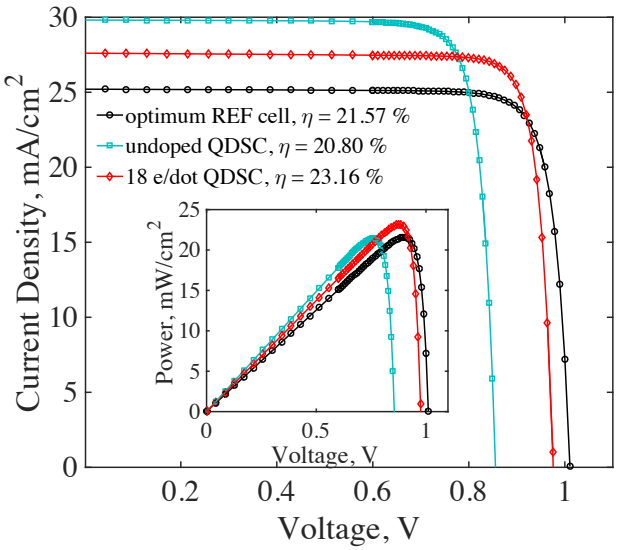

Fig. 9. $J-V$ characteristic under 1 sun AM1.5G illumination for optimum reference cell, undoped QD cell, and 18 e/dot QD cell, all in the thin-film light-trapping configuration. The inset shows the corresponding Power-Voltage curves.

quantum dot solar cells. Doping substantially reduces the fast carrier capture and recombination through QD states and allows the QD cell to achieve high open circuit voltage, comparable to the single-junction cell, while light trapping provides a substantial enhancement of QD photogeneration. Thus, even under dominant thermal escape operation, InAs/GaAs quantum dot solar cells might achieve higher efficiency than regular single-junction GaAs cells.

ACKNOWLEDGMENT

Research was supported by the Army Research Laboratory under Cooperative Agreement Number W911NF-14-2-0040, and by the European Union's Horizon 2020 research and innovation program, under Grant Agreement 687253 - TFQD. The views and conclusions contained in this document are those of the authors and should not be interpreted as representing the official policies, either expressed or implied, of the Army Research Laboratory or the U.S. Government or the European Commission. The U.S. Government is authorized to reproduce and distribute reprints for Government purposes notwithstanding any copyright notation herein.

REFERENCES

[1] A. Luque and A. Martí, "Increasing the efficiency of ideal solar cells by photon induced transitions at intermediate levels," *Phys. Rev. Lett.*, vol. 78, no. 26, pp. 5014–5017, 1997.

[2] K. X. Wang, Z. Yu, V. Liu, Y. Cui, and S. Fan, "Absorption enhancement in ultrathin crystalline silicon solar cells with antireflection and light-trapping nanocone gratings," *Nano letters*, vol. 12, no. 3, pp. 1616–1619, 2012.

[3] A. Mellor, A. Luque, I. Tobías, and A. Martí, "The feasibility of high-efficiency inas/gaas quantum dot intermediate band solar cells," *Solar Energy Materials and Solar Cells*, vol. 130, pp. 225–233, 2014.

[4] A. Sablon, J. W. Little, V. Mitin, A. Sergeev, N. Vagidov, and K. Reinhardt, "Strong enhamcement of solar cell efficiency due to quantum dots with built-in charge," *Nano Letters*, vol. 11, pp. 2311–2317, 2011.

[5] A. Martí, N. López, E. Antolin, E. Cánovas, C. Stanley, C. Farmer, L. Cuadra, and A. Luque, "Novel semiconductor solar cell structures: The quantum dot intermediate band solar cell," *Thin Solid Films*, vol. 511, pp. 638–644, 2006.

[6] Y. Okada, T. Morioka, K. Yoshida, R. Oshima, Y. Shoji, T. Inoue, and T. Kita, "Increase in photocurrent by optical transitions via intermediate quantum states in direct-doped inas/ganas strain-compensated quantum dot solar cell," *Journal of Applied Physics*, vol. 109, no. 2, p. 024301, 2011.

[7] M. Gioannini, A. Cedola, N. Di Santo, F. Bertazzi, and F. Cappelluti, "Simulation of quantum dot solar cells including carrier intersubband dynamics and transport," *IEEE J. Photovoltaics*, vol. 3, no. 4, pp. 1271–1278, Oct 2013.

[8] F. Cappelluti, M. Gioannini, and A. Khalili, "Impact of doping on inas/gaas quantum-dot solar cells: a numerical study on photovoltaic and photoluminescence behavior," *Solar Energy Materials and Solar Cells*, vol. -, no. -, pp. –, to appear, 2016.

[9] S. Polly, D. Forbes, K. Driscoll, S. Hellstrom, and S. Hubbard, "Delta-doping effects on quantum-dot solar cells," *IEEE J. Photovoltaics*, vol. 4, no. 4, pp. 1079–10 857, 2014.

[10] P. Lam, S. Hatch, J. Wu, M. Tang, V. G. Dorogan, Y. I. Mazur, G. J. Salamo, I. Ramiro, A. Seeds, and H. Liu, "Voltage recovery in charged inas/gaas quantum dot solar cells," *Nano Energy*, vol. 6, pp. 159 – 166, 2014.

[11] J. M. Gee, "The effect of parasitic absorption losses on light trapping in thin silicon solar cells," in *Photovoltaic Specialists Conference, 1988., Conference Record of the Twentieth IEEE*, Sept 1988, pp. 549–554 vol.1.

[12] M. A. Green, "Lambertian light trapping in textured solar cells and light-emitting diodes: analytical solutions," *Progress in Photovoltaics: Research and Applications*, vol. 10, no. 4, pp. 235–241, 2002.